ARTICLE

Journal homepage: www.the-innovation.org/energy-use

Energy Use

INNOVATION PRESS

Energy Use 1 (2026):100045

Contents lists available at INNOVATION PRESS

Sustainable Working Fluid Optimization for EORC-CCHP Systems: Low-GWP Mixtures, Thermodynamic Performance, and Exergy Analysis

Tao Yang,[1,*] Junbang Yao,[2] Xiaojing Li,[2] Qibin Li,[3] Baomin Dai,[4] Yulong Song,[5] Yifan Zhang,[6] Zilong Wang,[7] Shuang Wang,[8] Jian Li,[1] and Jun Shen[1,*]

*Correspondence: yangtao@bit.edu.cn (T. Y.); jshen@bit.edu.cn (J. S.)

Received: March 16, 2026; Accepted: March 24, 2026; Published Online: March 26, 2026; https://doi.org/10.59717/ipj.energy-use.2025.100045

GRAPHICAL ABSTRACT

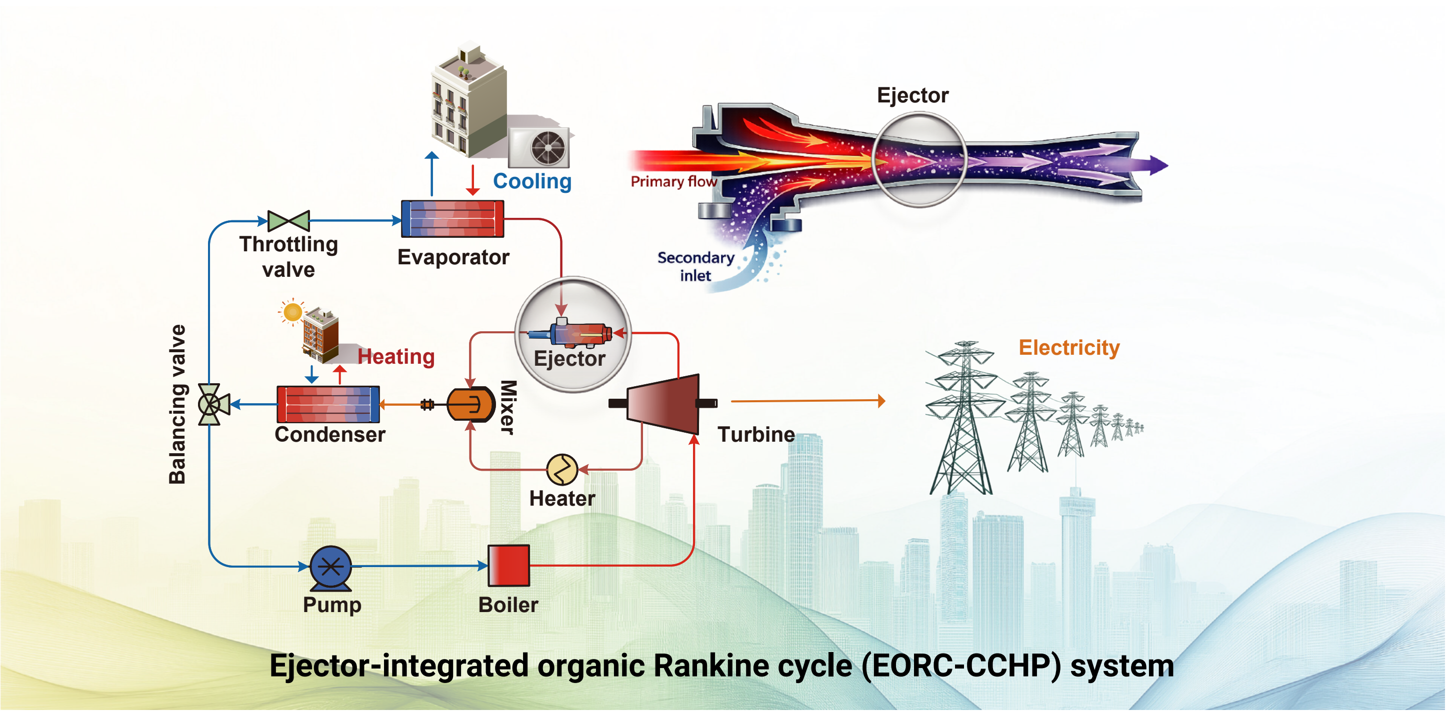

PUBLIC SUMMARY

- Proposed an ejector-integrated organic Rankine cycle (EORC-CCHP) system for efficient low-grade thermal energy use.
- Developed a framework combining refrigerant selection and thermodynamic optimization with a focus on sustainability.
- Identified R290/R1234yf as the optimal fluid, achieving a COPsys of 1.435.
- Parametric analysis revealed trade-offs in power and cooling outputs.
- Exergy analysis highlighted boiler and ejector as key areas for performance improvement.

ARTICLE

OPEN ACCESS

Journal homepage: www.the-innovation.org/energy-use

Energy Use

INNOVATION PRESS

Energy Use 1 (2026):100045

Contents lists available at INNOVATION PRESS

Sustainable Working Fluid Optimization for EORC-CCHP Systems: Low-GWP Mixtures, Thermodynamic Performance, and Exergy Analysis

Tao Yang,[1,*] Junbang Yao,[2] Xiaojing Li,[2] Qibin Li,[3] Baomin Dai,[4] Yulong Song,[5] Yifan Zhang,[6] Zilong Wang,[7] Shuang Wang,[8] Jian Li,[1] and Jun Shen[1,*]

[1]National Key Laboratory of Multi-perch Vehicle Propulsion Systems, School of Mechanical Engineering, Beijing Institute of Technology, Beijing 100081, China

[2]Hebei Key Laboratory of Low Carbon and High Efficiency Power Generation Technology, North China Electric Power University, Baoding 071003, China

[3]Key Laboratory of Low-grade Energy Utilization Technologies & Systems, Ministry of Education, Chongqing University, School of Energy and Power Engineering, Chongqing 400044, China

[4]Tianjin Key Laboratory of Refrigeration Technology, Tianjin University of Commerce, Tianjin 300134, China

[5]School of Energy and Power Engineering, Xi'an Jiaotong University, Xi'an 710049, China

[6]Xi'an Thermal Power Research Institute Co., Ltd. Xi'an 710032, China

[7]School of Energy and Power Engineering, University of Shanghai for Science and Technology, Shanghai 200093, China

[8]School of Engineering, Australian National University, Canberra ACT 0200, Australia

*Correspondence: yangtao@bit.edu.cn (T. Y.); jshen@bit.edu.cn (J. S.)

Received: March 16, 2026; Accepted: March 24, 2026; Published Online: March 26, 2026; https://doi.org/10.59717/ipj.energy-use.2025.100045

Citation: Yang T., Yao J., Li X., et al. (2026). Sustainable Working Fluid Optimization for EORC-CCHP Systems: Low-GWP Mixtures, Thermodynamic Performance, and Exergy Analysis. *Energy Use* **2**:100045.

Sustainable utilization of low-grade thermal energy is essential for advancing low-carbon distributed energy systems. This study proposes an ejector-integrated organic Rankine cycle combined cooling, heating and power (EORC-CCHP) system, in which ejector-based internal energy cascading is employed to reduce throttling losses and enhance system performance under low-temperature heat sources. A systematic framework integrating environmentally sustainable refrigerant selection and thermodynamic optimization is developed. Candidate working fluids, including R290, R600a, R1234yf, R1233zd(E), and their mixtures, are first screened from an environment perspective using total equivalent warming impact (TEWI) and life-cycle assessment (LCA). A comprehensive thermodynamic model is then established, and a multi-criteria decision-making approach based on TOPSIS is applied to assess system performance across multiple indicators. The results identify the R290/R1234yf mixture as the optimal working fluid, achieving a maximum closeness coefficient of 0.745 at an R290 mass fraction of 0.4, corresponding to a system coefficient of performance (COP_{sys}) of 1.435. Parametric analysis reveals that system performance is governed by coupled trade-offs among operating parameters: increasing boiler temperature enhances power output but introduces additional thermodynamic irreversibility, while variations in mass flow rate and ejector geometry redistribute energy utilization between power and cooling outputs. Exergy analysis shows that irreversibility is dominated by the boiler and ejector, which together account for the majority of exergy destruction, identifying them as key targets for performance improvement. This work demonstrates that the synergistic design of low-GWP refrigerant mixtures and ejector-enhanced thermodynamic cycles provides an effective pathway for improving the efficiency and sustainability of CCHP systems utilizing low-grade thermal energy.

INTRODUCTION

Improving the utilization efficiency of low-grade thermal energy has become a key pathway toward sustainable and low-carbon energy systems. A substantial amount of recoverable energy is available from industrial waste heat, geothermal resources, and solar thermal systems. However, its effective conversion remains challenging due to inherent thermodynamic limitations at low temperature levels.[1,2] Combined cooling, heating, and power (CCHP) systems have attracted increasing attention as an effective solution for distributed energy supply, as they enable cascade utilization of energy to simultaneously produce electricity, heating, and cooling. This integrated approach significantly enhances overall energy efficiency and contributes to carbon emission reduction. Nevertheless, the performance of conventional CCHP systems remains constrained under low-grade heat conditions, highlighting the need for advanced thermodynamic cycle design and system optimization.[3,4]

Among various thermodynamic cycles, the organic Rankine cycle (ORC) is widely recognized as an effective technology for recovering low- to medium-temperature heat sources due to its flexible working-fluid selection and favorable thermodynamic performance.[5,6] However, conventional ORC systems are primarily designed for power generation, and a considerable portion of residual heat is typically rejected to the environment, resulting in significant energy losses and limited overall efficiency, particularly under low-temperature conditions.[7,8] To address this limitation, ejector-integrated ORC configurations have been proposed. By replacing the throttling process with an ejector, part of the expansion work can be recovered to entrain secondary flow, thereby reducing exergy destruction and improving internal energy matching. In CCHP applications, the ejector-integrated ORC (EORC-CCHP) enables the simultaneous generation of electricity, heating, and cooling, where a fraction of turbine output is utilized to produce refrigeration without additional external energy input. This integration provides a promising pathway to enhance system efficiency and operational flexibility for low-grade heat utilization.[9-11]

Recent studies have explored various configurations of ejector-integrated ORC systems to improve cascade utilization of thermal energy. Yu et al.[12] demonstrated that incorporating dual-pressure evaporation and staged heat recovery significantly improves thermal matching and enhances both thermodynamic and economic performance which increases net power output by 23.6–40.6% and reduces total unit cost by 7.9–11.1%. Tang et al.[13] showed that replacing throttling valves with ejectors can effectively recover expansion work, thereby increasing exergy efficiency by 4.69–5.88 percentage points and net power output by 10.44–15.25%, while generating refrigeration without additional energy input. More advanced integrations have further coupled ejector-based ORC systems with other cycles to exploit multi-level energy utilization. For example, Du et al.[14] combined ejector-assisted ORC with a CO_2-based power cycle to simultaneously achieve efficient waste heat recovery and carbon emission reduction, while Niu et al.[15] demonstrated that integrating ejector ORC into Carnot battery systems can significantly enhance power output by over 30% and improve operational flexibility. Thus, ejector integration has been proven effective in reducing throttling losses, improving internal energy matching, and enabling flexible multi-energy outputs.

The selection of working fluids plays a decisive role in determining both the thermodynamic performance and environmental impact of ORC-based systems. With the implementation of the Kigali Amendment to the Montreal Protocol, high-global-warming-potential (GWP) refrigerants are being progressively phased down, accelerating the development of environmentally sustainable alternatives. Low-GWP working fluids, including natural hydrocarbons and hydrofluoroolefins (HFOs), have been extensively investigated. Hydrocarbons such as R290 and R600a exhibit excellent thermodynamic performance and ultra-low GWP but are constrained by flammability concerns,[16,17] whereas HFO refrigerants (e.g., R1234yf and R1233zd(E)) offer improved safety characteristics with relatively lower thermodynamic performance.[18,19] These trade-offs highlight the limitations of single-component working fluids in achieving optimal thermodynamic matching under varying operating conditions.[20] To overcome these limitations, refrigerant mixtures have been proposed as an effective strategy to tailor thermophysical properties and temperature glide, thereby improving heat transfer matching and overall system performance. Previous studies have demonstrated that mixed refrigerants can significantly enhance ORC efficiency and expand the operating range, particularly under variable heat source conditions.[21] However, most existing research has focused on conventional ORC systems, while the interaction between refrigerant mixtures and advanced ejector-integrated configurations remains insufficiently understood.

Therefore, although previous studies have investigated ORC-based CCHP systems, ejector-enhanced cycles, and low-GWP refrigerants independently, a critical research gap remains in their integrated optimization. Due to the inherent trade-offs among thermodynamic efficiency, environmental impact, and economic performance, multi-objective optimization methods have been widely adopted. Recent studies, have introduced advanced optimization algorithms,[22] such as NSGA-II[23] and multi-objective particle swarm optimization (MOPSO),[24] into ejector-integrated ORC-based systems. These studies demonstrate that multi-objective frameworks can effectively balance competing performance indicators and identify optimal operating conditions, and reveal strong coupling relationships among system configuration, working fluid properties, and operating parameters. In particular, systematic evaluations of emerging low-GWP refrigerant mixtures in EORC-CCHP systems are still limited, the coupled effects of refrigerant composition and operating parameters have not been fully elucidated, and the integration of exergy analysis into multi-objective optimization frameworks remains insufficient. These limitations hinder the development of efficient and environmentally sustainable system designs.

To address these challenges, this study presents a comprehensive investigation of an ejector-integrated ORC-based CCHP (EORC-CCHP) system using low-GWP refrigerant mixtures, with a focus on the coupling among working fluid properties, system configuration, and operating conditions. The main contributions are summarized as follows:

(1) A coupled environmental–thermodynamic evaluation framework based on TEWI and life-cycle assessment (LCA) is established to systematically screen low-GWP refrigerant mixtures.

(2) The influence of zeotropic mixture temperature glide on the synergistic production of power, heating, and cooling is elucidated, and the optimal working fluid (R290/R1234yf) and composition are identified.

(3) A coordinated optimization of key operating and structural parameters is conducted to determine optimal operating ranges and enhance overall system performance.

(4) An exergy-based analysis is performed to quantify and rank system irreversibility, identifying dominant sources of exergy destruction and key targets for performance improvement.

Through this integrated approach, the present study establishes a systematic framework for coupling working fluid design, thermodynamic cycle configuration, and multi-objective optimization, providing valuable guidance for the efficient and environmentally sustainable utilization of low-grade thermal energy.

MATERIALS AND METHODS

System description

Figure 1 illustrates the schematic diagram and corresponding *T*-*s* diagram of the proposed EORC-CCHP system. The working fluid leaving the boiler at high temperature and pressure (State 1) expands in the turbine to generate power. A split-flow configuration is adopted in the turbine: a portion of the fluid is extracted at an intermediate pressure (State 2) and directed to the ejector as the primary flow, while the remaining fluid continues to expand to a lower pressure (State 3), thereby maximizing power output. The low-pressure fluid (State 3) subsequently enters the heater, where a rated heating capacity of 5 kW is delivered (State 5). After heat release, this stream is directed to the mixer. Meanwhile, the intermediate-pressure stream (State 2) expands through the ejector nozzle, generating a high-velocity jet that creates a suction effect, entraining the secondary flow from the evaporator (State 9). The mixed flow passes through the diffuser, where pressure is partially recovered before exiting the ejector (State 4). The ejector outlet stream mixes with the heated stream and then enters the condenser (State 6), where heat is rejected to the surroundings. The condensed liquid flows to a balancing valve (State 7), where it is divided into two streams. One stream is throttled and enters the evaporator (State 8), absorbing environmental heat and vaporizing to State 9, thus completing the refrigeration cycle. The other stream is pressurized by the pump (State 10) and returned to the boiler, completing the power generation loop.

Refrigerant selection

The selection of working fluids plays a crucial role in determining the thermodynamic performance, environmental impact, and operational safety of EORC-CCHP systems, particularly under low-grade heat source conditions where thermophysical properties strongly influence heat transfer matching and cycle efficiency.[25] In this study, four representative low-GWP refrigerants (R290, R600a, R1234yf, and R1233zd(E)) are selected to capture the trade-offs among thermodynamic performance, environmental sustainability, and safety constraints. These pure fluids also serve as the basis for constructing zeotropic mixtures, enabling further investigation of composition-dependent thermodynamic behavior and system optimization. The key thermophysical and safety properties of the selected refrigerants are summarized in Table 1, providing the foundation for subsequent thermodynamic analysis and mixture design.

Thermodynamic model

This section establishes the thermodynamic model of the proposed EORC-CCHP system by providing a mathematical description of each component. To simplify the analysis, the following assumptions are adopted: (1) The system operates under steady-state conditions; (2) Pressure drops and heat losses in pipelines and components are neglected; (3) The working fluid is in a superheated state at the outlets of the boiler and evaporator; (4) The ejector operates under critical conditions, where the primary flow reaches a virtual throat and the secondary flow attains sonic velocity at the mixing section.

The ejector structure (Figure 1B), consists of a primary nozzle, suction chamber, mixing chamber, and diffuser. The ejector enhances system performance by replacing the throttling process and enabling energy recovery through momentum transfer between the primary and secondary flows. The high-pressure primary flow (State 2) expands through the nozzle, converting pressure energy into kinetic energy and forming a high-speed jet (State t). This jet induces a low-pressure region in the suction chamber, entraining the secondary flow from the evaporator (State 9). The two streams meet under critical mixing conditions and mix in the constant-area chamber, where a normal shock may occur, leading to a pressure rise and a transition from supersonic to subsonic flow. The mixed flow then enters the diffuser, where velocity decreases and pressure is recovered to the condenser level (State 4).

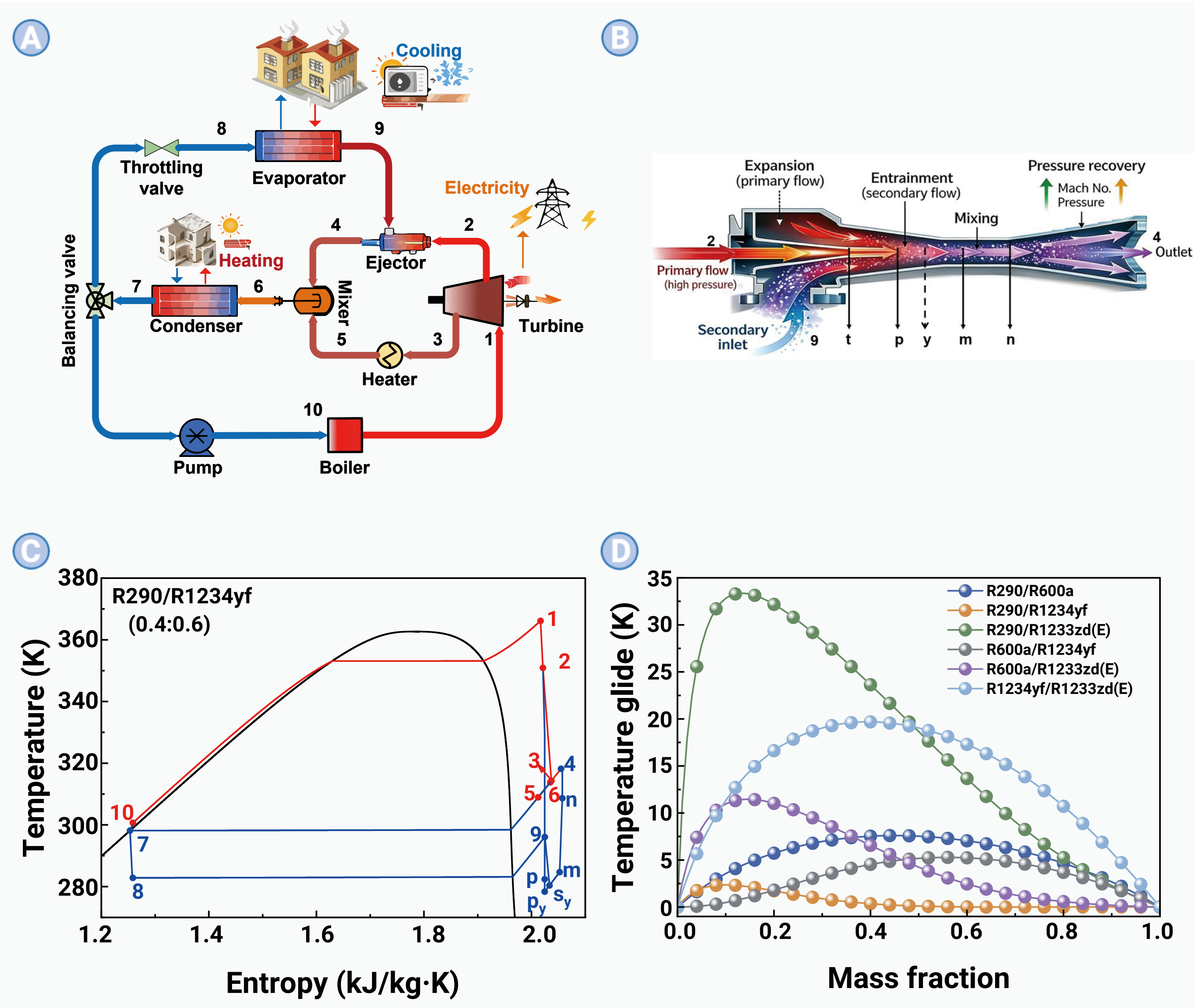

Figure 1. System parameter configuration diagram (A) Schematic of the EORC-CCHP system; (B) Structure diagram of the ejector; (C) T-s diagram of R290/R1234yf; (D) Temperature glide of different refrigerant mixtures.

The entrainment ratio (ER), defined as the ratio of the secondary mass flow rate to the primary mass flow rate, is a key performance indicator of the ejector:

$$ER = m_s/m_p \tag{1}$$

where m_s and m_p represent the mass flow rate of the secondary and primary flows, respectively.

The governing equations for each ejector section are summarized in Table 2 and are derived from the conservation of mass, momentum, and energy. The flow properties at the nozzle throat and other critical sections are obtained through iterative calculations that reconcile ideal isentropic relations with efficiency corrections, ensuring accurate representation of non-ideal behavior.

Environmental impact

To comprehensively evaluate the environmental performance of the system, both operational and life-cycle impacts are considered using the total equivalent warming impact (TEWI) and life cycle assessment (LCA) methods.

The TEWI accounts for both direct emissions (DE), caused by refrigerant leakage, and indirect emissions (IE), associated with energy consumption:[29]

$$TEWI = DE_{TEWI} + IE_{TEWI} \tag{2}$$

The direct emissions are calculated as:

$$DE_{TEWI} = C \cdot (L \cdot ALR + EOL) \cdot GWP_{100} \tag{3}$$

The indirect emissions are determined by:

$$IE_{TEWI} = L \cdot AEC \cdot EM \tag{4}$$

where C is the refrigerant charge (90 kg), L is the system lifetime (20 years), ALR is the annual leakage rate (5%), and EOL is the end-of-life leakage rate (85%). AEC is the annual energy consumption (8500 kWh), and EM is the carbon emission factor (0.6 kg CO_2/kWh).[30]

To further evaluate the overall environmental impact beyond operational emissions, LCA is conducted using the environmental impact potential (EIP) as the evaluation indicator. The LCA considers three stages of the system life cycle: (1) Manufacturing stage: environmental impacts associated with material production and component manufacturing (e.g., heat exchangers, turbines, and pumps); (2) Operation stage: impacts from refrigerant leakage (direct emissions) and energy consumption (indirect emissions); (3) Disposal

Table 1. Refrigerant safety parameters and thermophysical properties.[26-28]

Parameter	R290	R600a	R1234yf	R1233zd(E)
Molecular formula	C_3H_8	C_4H_{10}	$C_3H_2F_4$	$C_3H_2ClF_3$
Molecular weight	44.10	58.12	114.04	130.49
Normal boiling point (K)	231.036	261.401	243.665	291.413
Critical temperature (K)	369.89	407.81	367.85	439.60
Critical pressure (MPa)	4.251	3.629	3.382	3.624
ODP	0	0	0	0
GWP (100 years)	3.3	3	<1	7
Safety level	A3	A3	A2L	A1
Flammability classification	Higher Flammability LFL	Higher Flammability LFL	Lower Flammability LFL	No Flame Propagation
Burning rate (cm/s)	46	38	1.5	0
Minimum ignition energy (mJ)	0.25	0.25	5000-10000	No Flame Propagation
Lower explosive (vol% in air)	2.1	1.8	6.2	No Flame Propagation
Upper flammability limit (vol% in air)	9.5	8.4	12.3	No Flame Propagation

Table 2. Thermodynamic calculation equations for the ejector.

Stage	Equation	
Virtual throat	$V_{py} = \sqrt{2(h_p - h_{py}) + V_p^2}$	
	$A_{py} = \eta_{py} m_p / (\rho_{py} V_{py})$	
	$m_{ej} = m_s + m_p$	
Mixing chamber	$\phi_m (m_p V_{py} + m_s V_{sy}) = m_{ej} V_m$	
	$m_p(h_{py} + V_{py}^2/2) + m_s(h_{sy} + V_{sy}^2/2) = m_{ej}(h_m + V_m^2/2)$	
	$\rho_n A_a V_n = \rho_m A_a V_m$	
	$P_m - P_n = \rho_n V_n - \rho_m V_m$	
	$h_n + V_n^2/2 = h_m + V_m^2/2$	
Nozzle throat	Actual calculation equation	Ideal calculation equation
	$V_t = \sqrt{2(h_2 - h_t)}$	$V_{t,is} = \sqrt{2(h_2 - h_{t,is})}$
	$V_p = m_p / (\rho_p A_p)$	$V_p' = \sqrt{2(h_t - h_p) + V_t^2}$
	$V_{sy} = \sqrt{2(h_9 - h_{is})}$	$V_{sy,is} = \sqrt{2(h_9 - h_{sy,is})}$

stage: impacts related to refrigerant recovery/destruction and material recycling or landfill.

The EIP calculation for each stage is calculated as:

$$EIP_{man} = \sum_k M(k) \cdot Ef(k) \tag{5}$$

$$EIP_{op} = \sum_k \sum_i Q_i(k) \cdot Ef_i(k) + G(r) \tag{6}$$

$$EIP_{dis} = \sum_k M(k) \cdot Ef(k) \tag{7}$$

where k denotes the type of environmental impact (e.g., GWP, acidification potential (AP)); $M(k)$ represents material or energy consumption, $Q_i(k)$ is the emission of pollutant i, and $Ef_i(k)$ is the corresponding equivalent factor. $G(r)$ represents the environmental impact contribution of refrigerant r.

The total environmental impact over the life cycle is expressed as:

$$EIP_{total} = EIP_{man} + EIP_{op} + EIP_{dis} \tag{8}$$

To account for system performance, the life-cycle environmental impact per unit energy output is defined as:

$$EIP_{LCA} = \frac{EIP_{total}}{E_{total}} \tag{9}$$

where E_{total} is the total useful energy output of the system over its lifetime. The parameter values used in the above calculations are obtained from the literature.[31-33]

Evaluation criteria and modeling

Based on the thermodynamic and environmental frameworks established above, a comprehensive simulation model of the EORC-CCHP system is developed. The model integrates thermodynamic cycle analysis, ejector performance, and environmental evaluation to assess system behavior under varying operating conditions. The key design parameters and operating ranges are listed in Table 3. These parameters are selected to reflect practical operating conditions and to enable systematic analysis of the effects of geometric and thermodynamic variables on system performance.

The modeling workflow is illustrated in Figure 2. The governing equations of each component are solved iteratively to ensure conservation of mass, energy, and momentum throughout the system. For the ejector, the isentropic efficiencies of the primary flow, secondary flow, and mixed flow are assumed to be 92%, 85%, and 80%, respectively, with a mixing efficiency of 95%.[34] In addition, the isentropic efficiencies of the turbine and pump are set to 82% and 75%, respectively.[35] These values are adopted from the literature to account for irreversibility in practical systems.

Table 3. System design parameters and operating ranges.

Design parameters	Numerical
Main nozzle throat diameter (mm)	7.0-11.0
Main nozzle outlet diameter (mm)	11.85
Mixing chamber diameter (mm)	16.6
Expander outlet diameter (mm)	40
Evaporation temperature (°C)	10
Evaporation superheat (°C)	13
Condensing temperature (°C)	10~26
Boiler temperature (°C)	70-88
Boiler superheat (°C)	13
Boiler mass flow rate (kg/s)	0.5-1.5

RESULTS AND DISCUSSION

Environmental evaluation

To evaluate the environmental performance of the EORC-CCHP system using different low-GWP refrigerants, both operational and life-cycle impacts are assessed based on TEWI and LCA (including EIP indicators). This dual-perspective analysis enables a comprehensive comparison of refrigerants under increasingly stringent environmental regulations.

Figure 3A presents the TEWI values of the four refrigerants. It can be observed that, although all refrigerants exhibit zero ODP, significant differences in TEWI arise due to variations in GWP. Among the investigated refrigerants, R1234yf exhibits the lowest TEWI value (1.022×10^5 kg CO_2 eq), indicating the best overall carbon performance. R290 and R600a show comparable TEWI values (both approximately 1.025×10^5 kg CO_2 eq), primarily due to their extremely low GWP values. In contrast, R1233zd(E) yields a slightly higher TEWI (1.032×10^5 kg CO_2 eq), which can be attributed to its relatively higher GWP. The differences in TEWI are mainly governed by the direct emission term, highlighting the dominant role of refrigerant GWP in determining carbon-related environmental performance.

Figure 3B compares the environmental impact potentials (EIP) of different refrigerants across multiple indicators, including acidification potential (AP), eutrophication potential (EP), resource depletion potential (REP), and human toxicity potential (HTP). R290 and R600a demonstrate superior performance in terms of AP and EP. Specifically, the AP and EP values of R290 is 2.310×10^{-3} kg SO_2 eq and 8.908×10^{-4} kg NO_3^- eq, respectively. which are lower than those of R1234yf and R1233zd(E). This advantage is mainly attributed to the lower emissions of SO_2 and NO_X associated with hydrocarbon refrigerants during production and energy consumption stages. In contrast, R1233zd(E) exhibits slightly higher REP and HTP values compared to other refrigerants. This can be related to the presence of chlorine-containing components, which may contribute to increased environmental burdens during manufacturing and disposal processes.

Figure 3C illustrates the life-cycle GWP per unit energy output. R1233zd(E) exhibits the highest value (0.1400 kg CO_2 eq./ kWh), followed by R600a, R1234yf, and R290. This trend is consistent with the inherent GWP characteristics of the refrigerants and further confirms that GWP remains a key determinant of overall environmental impact.

Based on the combined analysis of TEWI and multiple EIP indicators, R1234yf and R290 emerge as the most promising candidates in terms of overall environmental performance. R1234yf shows a slight advantage due to its superior performance in GWP and HTP, making it particularly suitable for applications emphasizing carbon reduction and human health considerations. Meanwhile, R290 demonstrates outstanding performance in AP and EP, indicating its competitiveness in regions where acidification and eutrophication impacts are of primary concern. Therefore, R1234yf and R290 are recommended as priority working fluids for subsequent system optimization, provided that safety requirements and operational constraints are adequately addressed.

Thermodynamic performance

This section investigates the influence of refrigerant composition on system performance, including power efficiency, cooling efficiency, exergy efficiency, economic efficiency, Coefficient of Performance of Ejector Refrigeration (COP_{ref}) and COP_{sys}. The baseline operating conditions are set as follows: evaporation temperature of 10 °C, condensation temperature of 25 °C, boiler temperature of 80 °C, and refrigerant mass flow rate of 1 kg/s.

Figure 4A illustrates the variation of power efficiency with refrigerant composition. For most mixtures, the power efficiency exhibits a non-monotonic trend, initially decreasing and then increasing as the fraction of the first component increases. For example, the power efficiency of the R290/R600a mixture decreases from 9.65% to 7.05% and subsequently increases to 7.77%. This behavior can be attributed to the nonlinear variation of thermophysical properties in zeotropic mixtures, which affects turbine expansion characteristics and ejector performance. In particular, the matching between expansion ratio and critical properties plays a key role in determining power output. In contrast, the R290/R1233zd(E) mixture shows a monotonic increase in power efficiency, which is mainly due to the mismatch between its critical properties and the operating conditions at low R290 fractions, leading to suboptimal cycle performance in that region. As shown in Figure 4B, the cooling efficiency demonstrates more diverse trends depending on the refrigerant pair. For instance, the cooling efficiency of R290/R1234yf increases from 18.01% to 21.79% and then decreases to 18.39%, while that of R600a/R1234yf decreases monotonically. Conversely, the R290/R600a mixture exhibits a continuous increase in cooling efficiency. These differences are closely related to the temperature glide characteristics (Figure 1D), which affect heat transfer matching in the evaporator and condenser. When the temperature glide is better aligned with the heat source/sink profiles, the heat transfer process is enhanced, leading to improved cooling performance.

Figures 4C&D show the variations in exergy efficiency and economic efficiency, respectively. Both indicators exhibit trends similar to those of power and cooling efficiencies. The variation in exergy efficiency reflects the combined effect of irreversibility in key components, particularly the turbine and ejector. Improved matching of thermophysical properties reduces exergy destruction during expansion, mixing, and heat transfer processes. The economic efficiency is closely related to the overall energy output of the system, including power generation, cooling capacity, and heating output. Since the variation range of cooling efficiency is significantly larger than that of power efficiency, the economic efficiency is primarily governed by the cooling performance. For example, the exergy efficiency of the R290/R600a mixture decreases from 64.69% to 49.02% and then increases to 56.40%, while the economic efficiency shows a similar but less pronounced trend.

Figures 4E&F present the variations of COP_{ref} and COP_{sys}, respectively. The COP_{ref} generally exhibits a non-monotonic trend with composition. For the R290/R1234yf mixture, COP_{ref} decreases from 0.540 to 0.481 and then increases to 0.627. This behavior can be explained by the non-ideal mixing characteristics of refrigerants. At certain compositions, the thermophysical properties of the mixture lead to optimal coupling among the primary nozzle expansion, secondary flow entrainment, and mixing/diffusion processes in the ejector. Deviations from this optimal composition result in reduced performance. The variation of COP_{sys} follows a similar trend, as it is directly influenced by both power and cooling outputs. However, since the cooling contribution is dominant in the system, the trend of COP_{sys} is more closely aligned with that of cooling efficiency.

Figure 4G presents the TOPSIS-based closeness coefficient, which integrates multiple performance indicators. The R290/R1234yf mixture exhibits significantly higher closeness values compared to other refrigerant combinations, indicating superior overall performance. Specifically, when the mass fraction of R290 is 0.3–0.6, the closeness coefficients range from 0.723 to 0.745, with a maximum at approximately 0.4. This suggests that an optimal balance between thermodynamic performance and system efficiency can be achieved within this composition range. In comparison, other refrigerant combinations show lower closeness values, indicating less favorable trade-offs among the considered performance metrics. Based on the comprehensive evaluation, the R290/R1234yf mixture is selected for subsequent analysis. The composition range of R290 = 0.3–0.6 is identified as the optimal

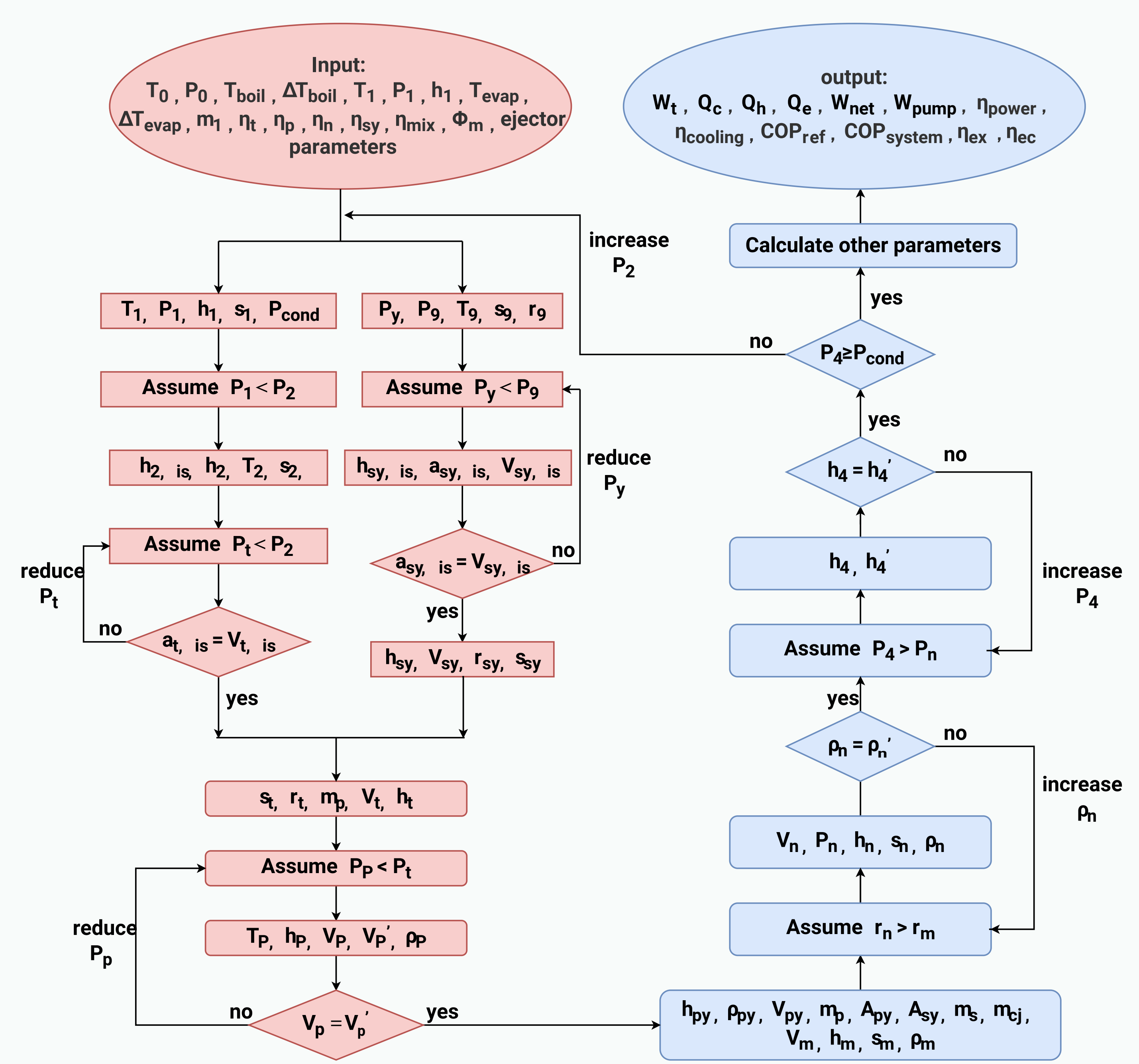

Figure 2. Schematic diagram of the EORC-CCHP system modeling process.

operating window for further system optimization.

Effect of boiler temperature

This section investigates the influence of boiler temperature (70–88 °C) on system performance under fixed evaporation temperature (10 °C), condensation temperature (25 °C), and refrigerant mass flow rate (1.0 kg/s).

Figure 5A shows the variation of net power output and cooling capacity with boiler temperature. The cooling capacity remains nearly constant across the investigated temperature range, with values of 51.51 kW, 56.76 kW, 60.94 kW, and 64.38 kW corresponding to R290 mass fractions of 0.3, 0.4, 0.5, and 0.6, respectively. This indicates that the cooling performance is weakly dependent on boiler temperature under the given operating conditions. In contrast, the net power output increases approximately linearly with increasing boiler temperature. For example, at 80 °C, the net power outputs for the four compositions are 15.78 kW, 17.79 kW, 19.89 kW, and 22.09 kW, respectively, increasing with the R290 fraction. This trend can be explained by the rise in turbine inlet temperature and pressure at higher boiler temperatures, which increases the specific enthalpy drop during expansion. Although the pump power consumption also increases slightly, its contribution is negligible compared to the gain in turbine output, leading to a net increase in system power.

Figure 5B illustrates the variation of heating capacity and boiler heat input. As the boiler temperature increases, the heating capacity exhibits a slight decreasing trend. This is primarily due to a reduction in mass flow rate through the condenser, which offsets the increase in enthalpy difference across the heating process. In contrast, the boiler heat input increases monotonically with temperature. For instance, when the R290 fraction varies from 0.3 to 0.6, the boiler heat input increases from 236.25–240.22 kW to 303.59–308.73 kW. This behavior results from the increasing enthalpy difference between the pump outlet and boiler outlet states as temperature rises.

Figure 5C presents the variation of exergy efficiency and economic efficiency. The economic efficiency increases monotonically with boiler temperature, mainly driven by the significant growth in net power output relative to the increase in heat input. In contrast, the exergy efficiency exhibits a single-

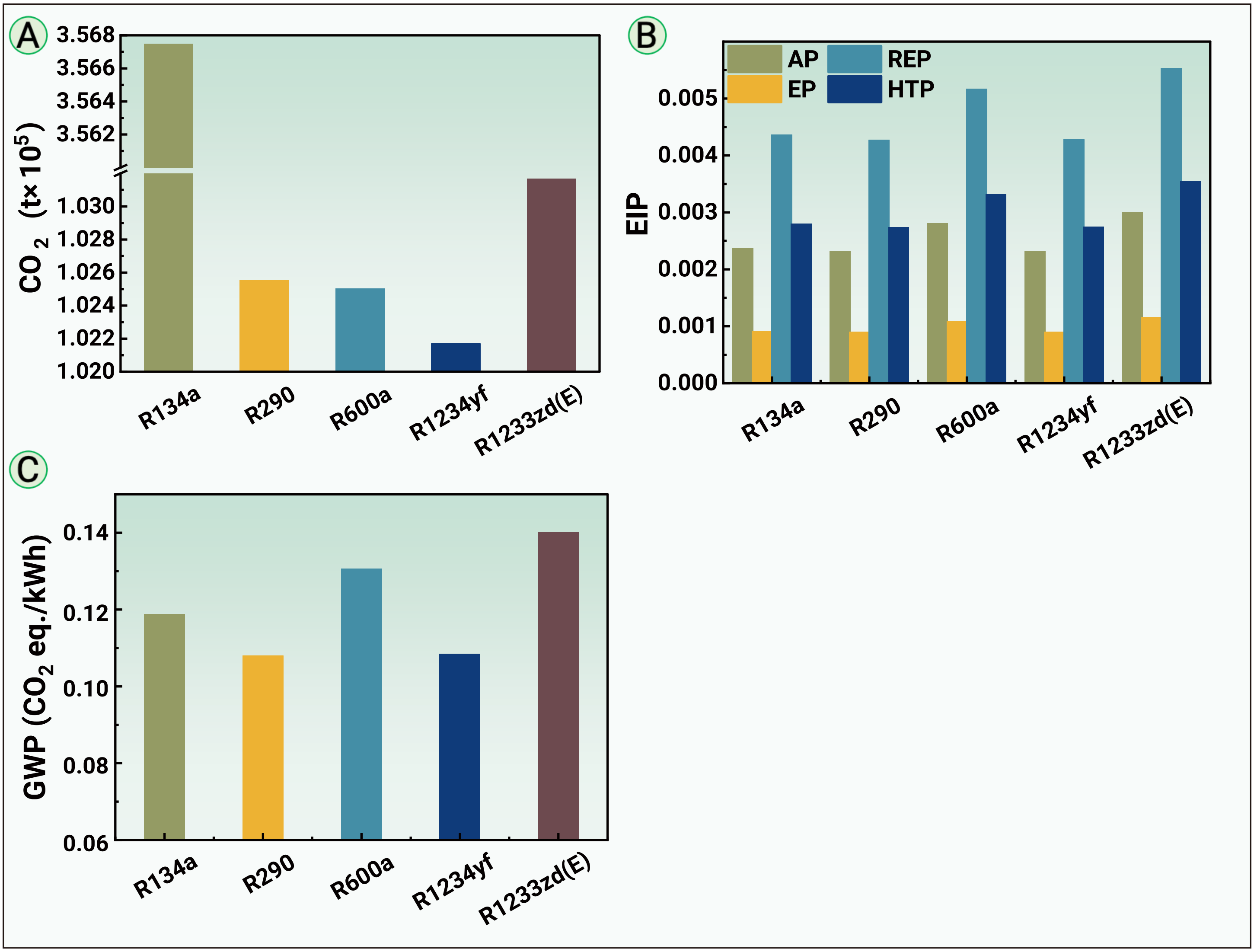

Figure 3. Environmental impact assessment of refrigerants (A) comparison of TEWI, (B) EIP and (C) GWP.

peak (unimodal) trend. At lower temperatures, increasing boiler temperature improves turbine performance and reduces the relative impact of exergy losses, leading to higher exergy efficiency. However, at higher temperatures, the irreversibility of heat transfer in the boiler becomes more pronounced, causing a rapid increase in exergy destruction. As a result, the overall exergy efficiency decreases beyond a certain temperature. This behavior reflects the trade-off between improved energy conversion and increased thermodynamic irreversibility at elevated temperature levels.

Figure 5D shows the variation of power efficiency and cooling efficiency. The power efficiency increases linearly with boiler temperature for all refrigerant compositions. For example, as the R290 fraction decreases from 0.6 to 0.3, the power efficiency increases from 5.83% to 8.10%, 5.68% to 7.91%, 5.50% to 7.71%, and 5.27% to 7.49%, respectively. This trend is consistent with the increase in net power output relative to heat input. Conversely, the cooling efficiency decreases with increasing boiler temperature. Since the cooling capacity remains nearly constant while the heat input increases significantly, the ratio defining cooling efficiency decreases.

Overall, increasing boiler temperature enhances power output and economic performance, while slightly reducing cooling efficiency and introducing additional exergy losses at higher temperature levels. Therefore, an optimal boiler temperature exists that balances power generation and thermodynamic efficiency, which should be considered in practical system operation.

Effect of refrigerant mass flow rate

This section investigates the influence of refrigerant mass flow rate in the boiler, varying from 0.5 kg/s to 1.5 kg/s, on the thermodynamic, exergy, and economic performance of the system.

Figure 6A presents the variation of mass flow rates within the ejector. It can be observed that the primary flow rate, secondary flow rate, and entrainment ratio remain nearly constant as the boiler mass flow rate increases. This behavior is attributed to the geometric constraints of the ejector and the critical flow conditions. Under choked flow conditions, the mass flow rates of the primary and secondary streams are primarily determined by nozzle geometry and thermodynamic state rather than upstream mass flow variations. Consequently, the entrainment ratio remains constant at approximately 0.6822. However, the increase in total system mass flow rate leads to a redistribution of flow in other components. In particular, the mass flow rate after the second-stage expansion of the turbine increases significantly (e.g., m_3 has increased from 0.118 kg/s to 1.118 kg/s), while the total mass flow rate entering the condenser increases accordingly.

Figures 6B-D illustrate the variations in net power output, heating capacity, and boiler heat input. All three quantities increase monotonically with increasing mass flow rate. The increase in net power output is primarily due to the rise in mass flow participating in the secondary expansion of the turbine. Since the primary extraction flow remains constant, additional mass flow contributes directly to work generation, resulting in a significant increase in turbine output. The increase in net power output is primarily due to the rise in mass flow participating in the secondary expansion of the turbine. Since the primary extraction flow remains constant, additional mass flow contributes directly to work generation, resulting in a significant increase in turbine output.

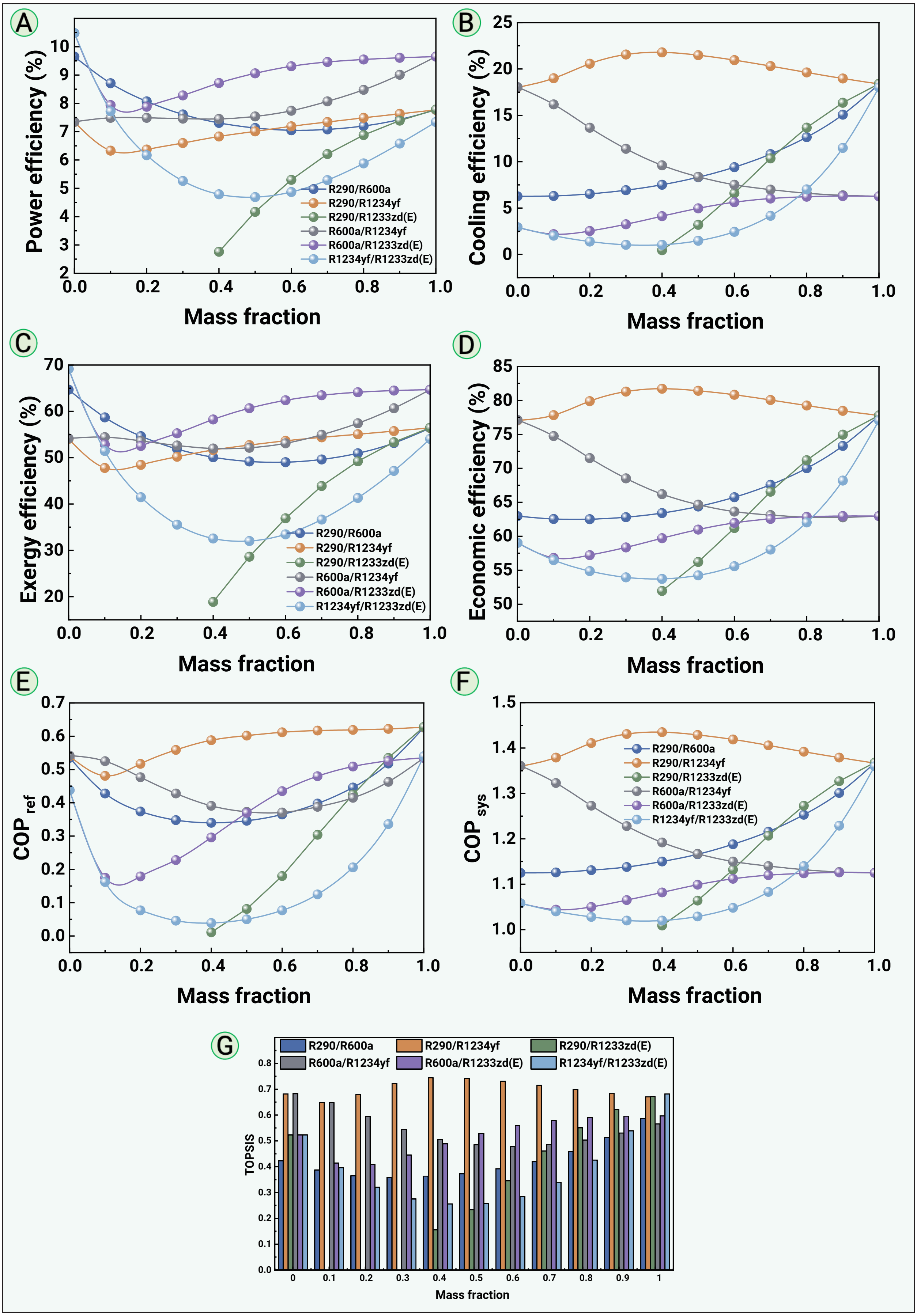

Figure 4. Effect of refrigerant composition on (A) power efficiency, (B) cooling efficiency, (C) exergy efficiency, (D) economic efficiency, (E) COP_{ref} and (F) COP_{sys} and (G) TOPSIS analysis.

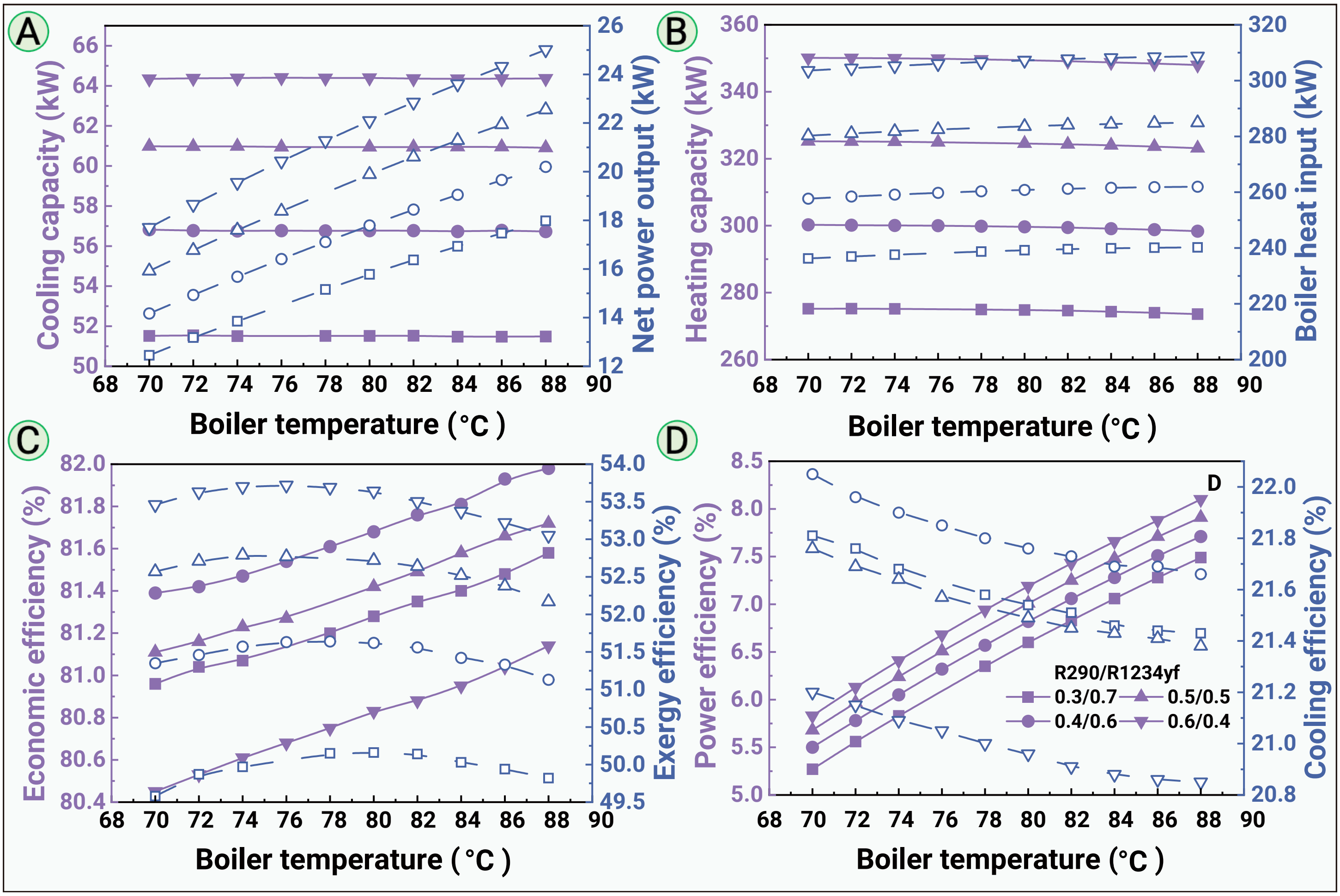

Figure 5. Effect of boiler temperature on the (A) cooling capacity and net power output, (B) heating capacity and boiler heat input, (C) economic efficiency and exergy efficiency, and (D) power efficiency and cooling efficiency.

Figures 6E-I show the influence of mass flow rate on key performance indicators, including heat recovery ratio, power efficiency, cooling efficiency, economic efficiency, and exergy efficiency. A notable feature is the scaling effect observed in the system: as mass flow rate increases, most energy-related quantities (power, heating, cooling, and heat input) scale approximately proportionally. As a result, some performance indicators exhibit relatively weak sensitivity to mass flow rate. Specifically, the heat recovery ratio, cooling efficiency, and economic efficiency show similar decreasing trends. This is because, although useful outputs increase, the corresponding increase in heat input is proportionally larger, leading to reduced efficiency metrics. For example, at an R290 fraction of 0.6, the heat recovery ratio decreases from 0.971 to 0.928, the cooling efficiency decreases from 41.93% to 13.98%, and the economic efficiency decreases from 106.53% to 72.27%. In contrast, the power efficiency increases with mass flow rate. For instance, at an R290 fraction of 0.6, the power efficiency rises from 4.09% to 8.22%. This is because the additional mass flow contributes more significantly to turbine work than to heat input, resulting in improved power conversion efficiency.

Figure 6I shows that the exergy efficiency increases with mass flow rate for all refrigerant compositions. For example, at an R290 fraction of 0.4, the exergy efficiency increases from 37.38% to 56.23%. This improvement can be attributed to enhanced utilization of available energy as the system throughput increases. Higher mass flow rates reduce the relative impact of fixed irreversibility in components, leading to improved overall exergy efficiency. Additionally, at the same mass flow rate, higher R290 fractions result in higher exergy efficiency. For example, at 1.0 kg/s, the exergy efficiencies decrease from 53.64% to 50.17% as the R290 fraction decreases, indicating better thermodynamic matching at higher R290 content.

Overall, increasing the refrigerant mass flow rate enhances the absolute energy outputs of the system, including power generation and heating capacity. However, due to scaling effects, some efficiency indicators decrease, while power and exergy efficiencies improve. This suggests that the mass flow rate is a key operational parameter that governs the trade-off between energy output and efficiency, and should be optimized according to specific application requirements.

Effect of ejector nozzle throat diameter

This section investigates the influence of the ejector primary nozzle throat diameter (7.0–11.0 mm) on system performance. The operating conditions are fixed at a boiler temperature of 80 °C, evaporation temperature of 10 °C, condensation temperature of 25 °C, and refrigerant mass flow rate of 1.0 kg/s.

Figure 7A shows the variation of the entrainment ratio with nozzle throat diameter. The entrainment ratio decreases monotonically as the throat diameter increases for all refrigerant compositions. For example, when the R290 fraction decreases from 0.6 to 0.3, the entrainment ratio drops from 0.832 to 0.360, 0.823 to 0.356, 0.805 to 0.348, and 0.773 to 0.330, respectively. This behavior can be explained by the reduction in jet velocity at larger nozzle diameters. Under choked flow conditions, increasing the throat diameter reduces the flow acceleration and exit velocity of the primary jet, thereby weakening the momentum transfer to the secondary flow. As a result, the suction capacity of the ejector decreases, leading to a lower entrainment ratio.

Figures 7B-D illustrate the variations in heating capacity, cooling capacity, and net power output. Both heating and cooling capacities decrease with increasing nozzle throat diameter, whereas the net power output shows an increasing trend. The reduction in cooling and heating capacities is primarily attributed to the decline in entrainment ratio, which reduces the secondary flow rate and weakens the heat transfer processes in the evaporator and condenser. In contrast, the increase in net power output is related to changes

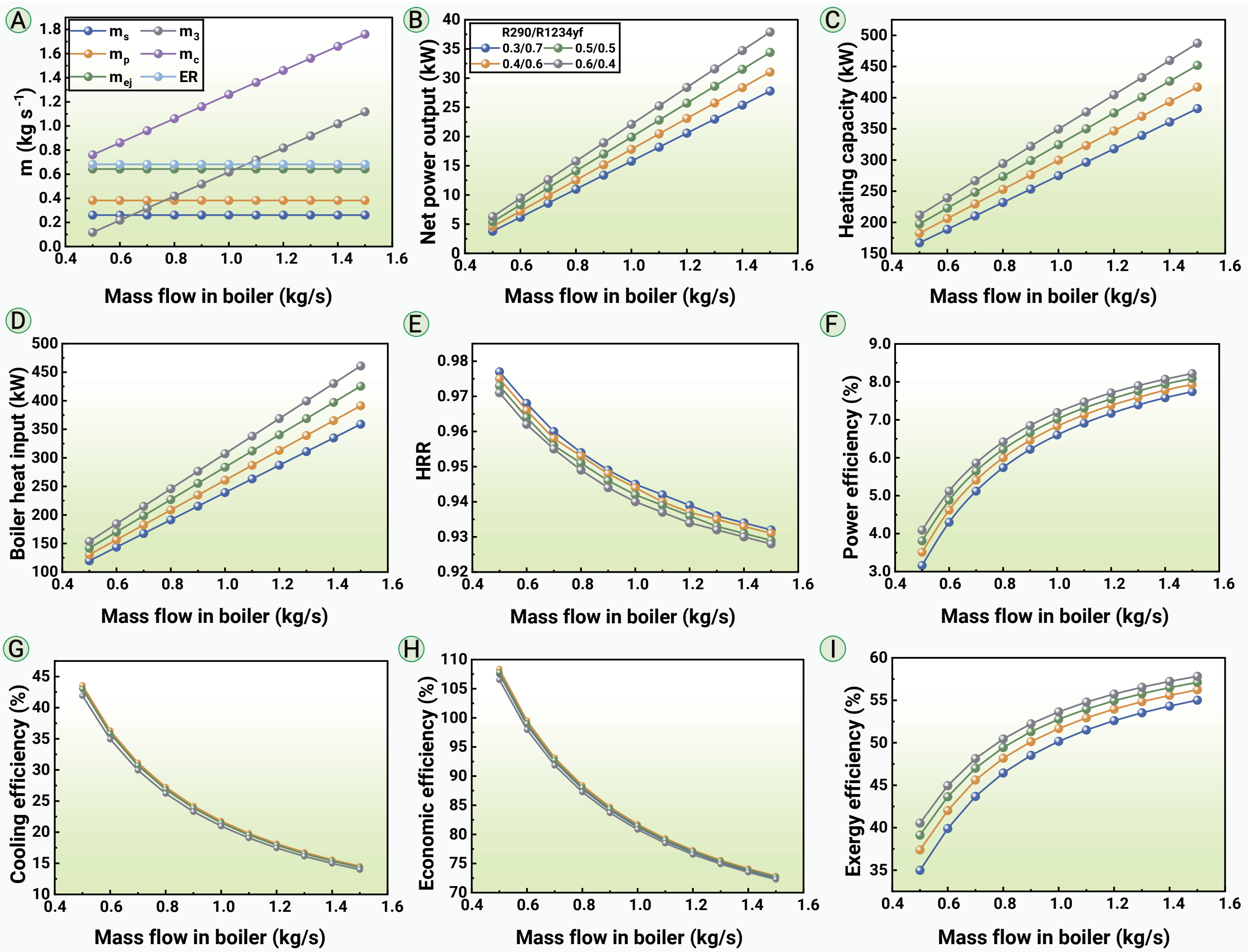

Figure 6. Influence of mass flow in the boiler on different parameters of the system.

in flow distribution within the system. As less mass flow is entrained into the ejector, a larger fraction of the working fluid undergoes turbine expansion, leading to increased work output.

Figures 7E-H present the variations in power efficiency, cooling efficiency, economic efficiency, and exergy efficiency. The power efficiency increases with nozzle diameter due to the enhanced turbine contribution to net work. For instance, when the R290 fraction varies from 0.6 to 0.3, the power efficiency increases from 6.98% to 7.80%, 6.81% to 7.65%, 6.61% to 7.49%, and 6.38% to 7.28%, respectively. In contrast, the cooling efficiency decreases with increasing nozzle diameter, consistent with the reduction in entrainment ratio and cooling capacity. As a result, the economic efficiency also decreases, since it is strongly influenced by the cooling and heating outputs. For example, at an R290 fraction of 0.6, the economic efficiency decreases from 82.79% to 72.41%. The exergy efficiency, however, increases with nozzle diameter. This indicates that, despite the reduction in cooling performance, the system achieves more efficient utilization of available energy due to improved power generation and reduced relative irreversibility in the expansion process.

Figure 7I shows the variation of COP_{ref}, which decreases significantly with increasing nozzle diameter. For example, at an R290 fraction of 0.6, COP_{ref} decreased from 0.709 to 0.323 as the diameter increases from 7.0 mm to 11.0 mm. This trend is directly linked to the decline in entrainment ratio. A larger nozzle diameter weakens the expansion intensity and velocity of the primary flow, reducing the suction capability and secondary flow rate. Consequently, the refrigeration capacity and overall performance of the ejector refrigeration subsystem deteriorate.

Overall, increasing the nozzle throat diameter enhances power generation and exergy efficiency but deteriorates cooling performance and economic efficiency. This reflects a fundamental trade-off between power-oriented and cooling-oriented operation modes. Therefore, the nozzle throat diameter should be carefully optimized based on the desired system objective. Smaller diameters are more suitable for applications prioritizing cooling performance, whereas larger diameters favor power generation and exergy efficiency.

System exergy analysis

To further reveal the distribution characteristics of irreversible losses within the EORC-CCHP system, an exergy analysis is conducted based on the second law of thermodynamics. The exergy destruction of each component is evaluated to identify the dominant sources of irreversibility and potential directions for system improvement.

Under the reference operating conditions, using the R290/R1234yf mixture with an R290 mass fraction of 0.4, the distribution of exergy losses among system components is presented in Figure 8. It can be observed that the boiler contributes the largest share of exergy destruction, accounting for 28.9% of the total exergy input. This is primarily due to the large temperature difference between the high-temperature heat source and the working fluid, which leads to significant irreversibility during heat transfer. This result indicates that improving heat transfer matching and reducing temperature gradients in the boiler are critical for enhancing overall system efficiency. The ejector is the second-largest source of exergy loss, contributing 26.2%. The high irreversibility in the ejector arises from complex internal processes, including rapid expansion, momentum exchange, shock waves, and non-

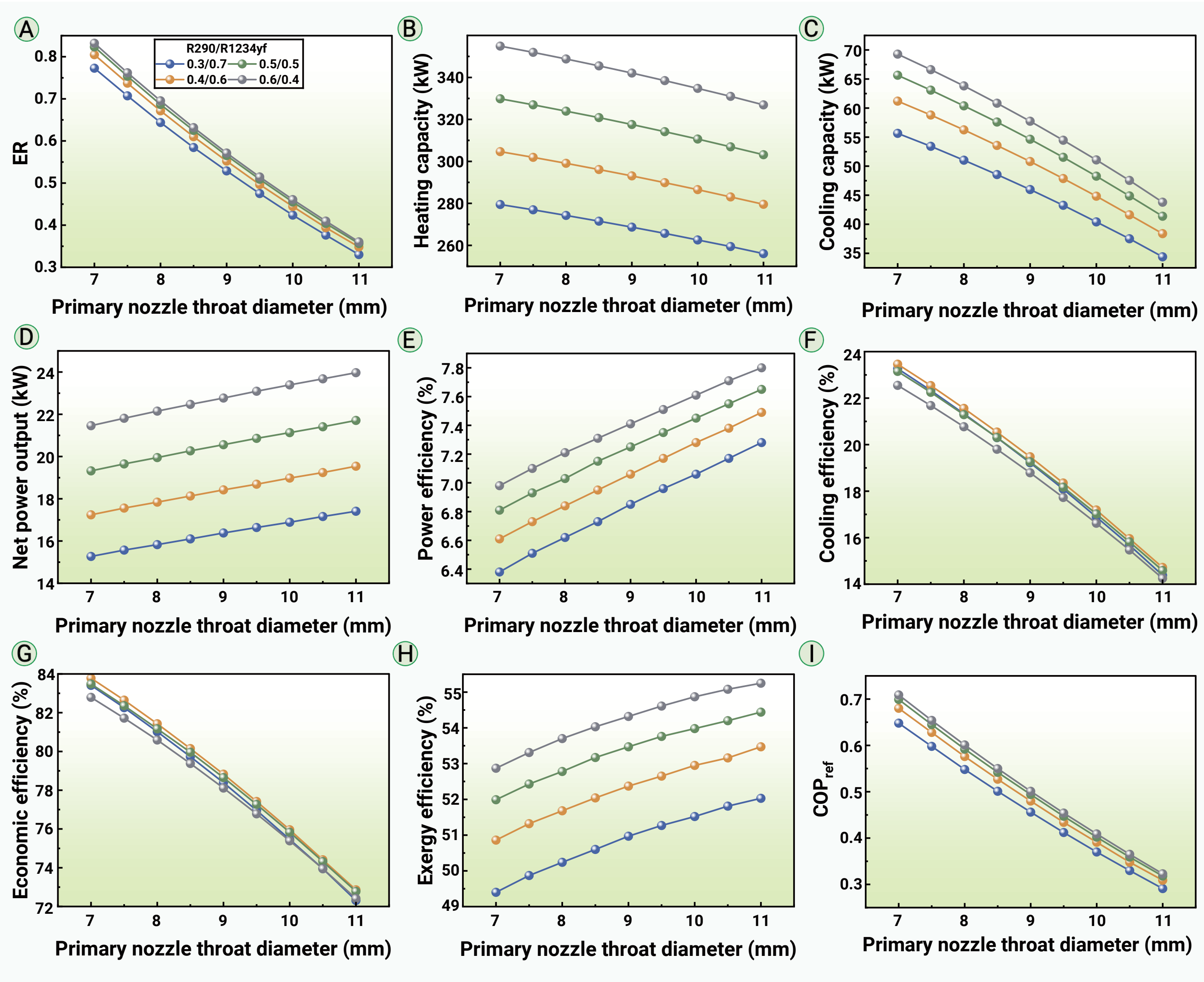

Figure 7. Influence of the throat diameter of the main nozzle on different parameters of the system.

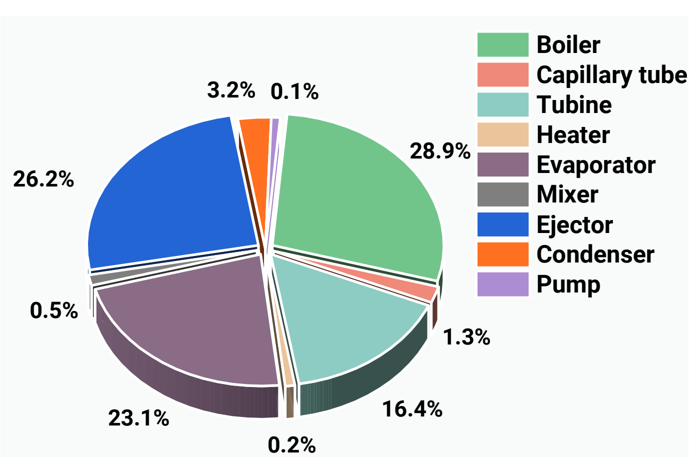

Figure 8. Exergy destruction proportion of each system component.

equilibrium mixing between primary and secondary flows. These processes inherently involve substantial entropy generation, making the ejector a key target for performance optimization. The evaporator accounts for 23.1% of the total exergy loss, mainly due to temperature differences between the working fluid and the heat source during phase change. Similar to the boiler, this highlights the importance of heat transfer matching in reducing thermodynamic losses. The turbine contributes 16.4% of the exergy destruction. Although it plays a central role in power generation, irreversible losses arise from non-ideal expansion, mechanical inefficiencies, and internal fluid friction, which limit the conversion of available energy into useful work. In contrast, the exergy losses associated with the mixer, throttle valve, pump, and heater are relatively small, with a combined contribution of less than 5%, indicating that their impact on overall system irreversibility is limited.

The exergy analysis reveals that more than 75% of the total irreversibility is concentrated in three components: the boiler, ejector, and evaporator. This indicates that system performance is primarily constrained by heat transfer processes and ejector-related flow irreversibility. From a design and optimization perspective, priority should be given to: improving heat transfer matching in the boiler and evaporator (e.g., through temperature glide matching of zeotropic mixtures), optimizing ejector geometry and operating conditions to reduce mixing and shock losses, and enhancing turbine efficiency to further improve energy conversion. Overall, the results demonstrate that reducing heat transfer irreversibility and improving ejector performance are the most effective pathways for enhancing the thermodynamic performance of the EORC-CCHP system.

CONCLUSIONS

This study systematically investigates the thermodynamic and exergy performance of an EORC-CCHP system using low-GWP refrigerant mixtures. The main findings can be summarized as follows:

(1) The R290/R1234yf mixture demonstrates superior overall performance among the investigated working fluids. An optimal composition is identified at an R290 mass fraction of around 0.4, where a balanced enhancement in power output, cooling capacity, and system efficiency is achieved.

(2) Boiler temperature primarily governs the trade-off between power output and thermodynamic irreversibility. Increasing temperature enhances turbine work output, but simultaneously intensifies heat transfer irreversibility, leading to an optimal operating range rather than a monotonic improvement in exergy efficiency.

(3) The refrigerant mass flow rate mainly affects the scale of energy throughput rather than intrinsic efficiency. While higher flow rates significantly increase system capacity, they introduce diminishing returns in energy utilization efficiency, highlighting a fundamental trade-off between capacity and performance.

(4) The ejector nozzle geometry plays a critical role in redistributing system performance. Enlarging the nozzle throat improves power and exergy efficiency by reducing internal flow losses, but weakens entrainment capability and cooling performance, indicating a structural trade-off between thermodynamic efficiency and refrigeration effectiveness.

(5) Exergy analysis reveals that system inefficiencies are dominated by heat transfer and mixing processes. More than 75% of total exergy destruction is concentrated in the boiler, ejector, and evaporator, identifying them as the primary bottlenecks limiting system performance.

From a system design perspective, optimal performance can be achieved by adopting R290/R1234yf mixtures with moderate R290 fractions (0.3–0.6), maintaining the boiler temperature within an intermediate range, and carefully optimizing ejector geometry. Future improvements should focus on reducing heat transfer irreversibility and enhancing ejector flow structure, which are identified as the most effective pathways for improving overall system efficiency.

Nomenclature

Symbols	
A	Cross-sectional area (m^2)
a	Acoustic velocity (m/s)
D	Diameter (m)
h	Enthalpy (J/kg)
m	Mass flow rate (kg/s)
P	Pressure (kPa)
Q	Heat transfer rate (kW)
s	Entropy (J/kg · K)
T	Temperature (°C)
V	Flow velocity (m/s)
Greek symbols	
β/α	Price ratio of cooling/heating to electricity per unit
Δ	Change in the value
η	Isentropic efficiency
ρ	Density (kg/m^3)
Subscripts	
0	Ambient
a	Constant area section
boil	Boiler
con	Condenser
y	Hypothetical throat section
e	Cooling
ec	Economic
eva	Evaporator
tur	Turbine
t	Primary nozzle throat
ex	Exergy
h	Heating
is	Isentropic
m	Mixing
n	Normal shock
p	Primary nozzle exit
ref	Refrigeration of ejector
sys	System
Abbreviations	
AP	Acidification potential
CCHP	Combined cooling, heating and power
COP	Coefficient of performance
EIP	Environmental impact potential
EORC-CCHP	Ejector-Integrated Organic Rankine Cycle combined cooling, heating and power
EERC	Ejector expansion refrigeration cycle
VCC	Vapor compression refrigeration cycle
EP	Eutrophication potential
GWP	Global warming potential
HRR	Heat recovery ratio
HTP	Human toxicity potential
LCA	Life cycle assessment
ODP	Ozone depletion potential
ORC	Organic Rankine cycle
REP	Respiratory effects potential

REFERENCES

1. Liu Y., Han B., Jiang CQ, et al. (2024). Uncovering the role of urban green infrastructure in carbon neutrality: A novel pathway from the urban green infrastructure and cooling power saving. *J. Clean. Produc.* **452**. DOI:10.1016/j.jclepro.2024.142193
2. Lalau Y., Al Asmi I., Olives R, et al. (2022). Energy analysis and life cycle assessment of a thermal energy storage unit involving conventional or recycled storage materials and devoted to industrial waste heat valorisation. *J. Clean. Product.* **330**. DOI:10.1016/j.jclepro.2021.129950
3. Huang S., Li J., Bai Z, et al. (2024). Assessment of the effect of heat storage on the production of clean geothermal energy using the medium and deep U-type borehole heat exchanger system. *J. Clean. Product.* **447**. DOI:10.1016/j.jclepro.2024.141471
4. Keskin I. and Soykan G. (2023). Distribution grid electrical performance and emission analysis of combined cooling, heating and power (CCHP)-photovoltaic (PV)-based data center and residential customers. *J. Clean. Product.* **414**. DOI:10.1016/j.jclepro.2023.137448
5. Norani M. and Deymi-Dashtebayaz M. (2022). Energy, exergy and exergoeconomic optimization of a proposed CCHP configuration under two different operating scenarios in a data center: Case study. *J. Clean. Product.* **342**. DOI:10.1016/j.jclepro.2022.130971
6. Hung TC., Shai TY. and Wang SK. (1997). A review of organic rankine cycles (ORCs)

for the recovery of low-grade waste heat. *Energy* **22**:661–667. DOI:10.1016/S0360-5442(96)00165-X

7. Bao J. and Zhao L. (2013). A review of working fluid and expander selections for organic Rankine cycle. *Renew. Sustain. Energy Rev.* **24**:325–342. DOI:10.1016/j.rser.2013.03.040
8. Wu D., Han S., Liu Z, et al. (2025). Multi-time-scale Optimized Operation Method for Integrated Energy Systems Considering Equipment Dynamic Performance. *Energy Use* **1**(1). DOI:10.59717/ipj.energy-use.2025.100012
9. Jafary S., Khalilarya S., Shawabkeh A, et al. (2021). A complete energetic and exergetic analysis of a solar powered trigeneration system with two novel organic Rankine cycle (ORC) configurations. *J. Clean. Product.* **281**. DOI:10.1016/j.jclepro.2020.124552
10. Dai Y., Wang J. and Gao L. (2009). Exergy analysis, parametric analysis and optimization for a novel combined power and ejector refrigeration cycle. *Appl. Therm. Eng.* **29**:1983–1990. DOI:10.1016/j.applthermaleng.2008.09.016
11. Wu J., Liang Y., Sun Z, et al. (2024). Dynamic analysis and control strategy of ORC coupled ejector expansion refrigeration cycle driven by geothermal water. *J. Clean. Product.* **445**. DOI:10.1016/j.jclepro.2024.141309
12. Yu W., Wang H. and Ge Z. (2021). Comprehensive analysis of a novel power and cooling cogeneration system based on organic Rankine cycle and ejector refrigeration cycle. *Energy Conver. Manage.* **232**. DOI:10.1016/j.enconman.2021.113898
13. Tang Z., Wu C., Liu C, et al. (2021). Thermodynamic analysis and comparison of a novel dual-ejector based organic flash combined power and refrigeration cycle driven by the low-grade heat source. *Energy Conver. Manage.* **239**. DOI:10.1016/j.enconman.2021.114205
14. Du Y-D., Li M-J. and Li H-Z. (2025). Thermodynamic and environmental performance assessment of an ejector-based organic Rankine cycle coupled with chemical looping combustion for combined cooling and power. *Energy* **336**. DOI:10.1016/j.energy.2025.138451
15. Niu J., Dong L., Wang J, et al. (2026). Optimization of system layout and working fluid selection based on genetic algorithm to improve Carnot battery performance. *Energy Conver. Manage.* **348**. DOI:10.1016/j.enconman.2025.120705.
16. Zheng B. and Weng YW. (2010). A combined power and ejector refrigeration cycle for low temperature heat sources. *Solar Energy* **84**:784–791. DOI:10.1016/j.solener.2010.02.001
17. Sarkar J. (2015). Review and future trends of supercritical CO2 Rankine cycle for low-grade heat conversion. *Renew. Sustain. Energy Rev.* **48**:434-451. hDOI:10.1016/j.rser.2015.04.039
18. McLinden MO., Kazakov AF., Steven Brown J, et al. (2014). A thermodynamic analysis of refrigerants: Possibilities and tradeoffs for Low-GWP refrigerants. *International J. Refrig.* **38**:80–92. DOI:10.1016/j.ijrefrig.2013.09.032
19. Invernizzi CM., Iora P., Preißinger M, et al. (2016). HFOs as substitute for R-134a as working fluids in ORC power plants: A thermodynamic assessment and thermal stability analysis. *Appl. Therm. Eng.* **103**:790–797. DOI:10.1016/j.applthermaleng.2016.04.101
20. Palm B. (2008). Hydrocarbons as refrigerants in small heat pump and refrigeration systems – A review. *Int. J. Refrig.* **31**:552–563. DOI:10.1016/j.ijrefrig.2007.11.016
21. Zhang Y., Song Y., Liu M, et al. (2025). The Innovative Application and Development Trend of CO₂ Thermodynamic Cycle Technology in the New Energy Structure system. *Energy Use*, **1**(2). DOI:10.59717/ipj.energy-use.2025.100028.
22. Pan D. and Gholami Farkoush S. (2023). Comprehensive analysis and multi-objective optimization of power and cooling production system based on a flash-binary geothermal system. *Appl. Therm. Eng.* **229**. DOI:10.1016/j.applthermaleng.2023.120398
23. Mortazavi H., Beni HM., Nadooshan AA, et al. (2024). 4E analysis and triple objective NSGA-II optimization of a novel solar-driven combined ejector-enhanced power and two-stage cooling (EORC-TCRC) system. *Energy* **294**. DOI:10.1016/j.energy.2024.130803
24. Pazuki M-M., Kolahi M-R., Ebadollahi M, et al. (2024). Enhancing efficiency in an innovative geothermal poly-generation system for electricity, cooling, and freshwater production through integrated multi-objective optimization: A holistic approach to energy, exergy, and enviroeconomic effects. *Energy* **313**. DOI:10.1016/j.energy.2024.133862
25. Yang T., Siepmann JI. and Wu J. (2021). Phase Equilibria of Difluoromethane (R32), 1,1,1,2-Tetrafluoroethane (R134a), and trans-1,3,3,3-Tetrafluoro-1-propene (R1234ze(E)) Probed by Experimental Measurements and Monte Carlo Simulations. *Ind. Eng. Chem. Res.* **60**:739–752. DOI:10.1021/acs.iecr.0c05442
26. Yaïci W. and Longo M. (2025). Ejector-enhanced air-source heat pump systems using ultra-low-GWP zeotropic mixtures in cold climates. *Energy* **328**. DOI:10.1016/j.energy.2025.136492
27. Eyerer S., Wieland C., Vandersickel A, et al. (2016). Experimental study of an ORC (Organic Rankine Cycle) and analysis of R1233zd-E as a drop-in replacement for R245fa for low temperature heat utilization. *Energy* **103**:660–671. DOI:10.1016/j.energy.2016.03.034
28. Yang T., Hu X., Meng X, et al. (2020). Vapour-liquid equilibria for the binary systems of pentafluoroethane {(R125) + 2,3,3,3-tetrafluoroprop-1-ene (R1234yf)} and {trans-1,3,3,3-tetrafluoropropene R1234ze(E)}. *J. Chem. Thermo.* **150**. DOI:10.1016/j.jct.2020.106222
29. Andrade A., Zapata-Mina J. and Restrepo A. (2024). Exergy and environmental assessment of R-290 as a substitute of R-410A of room air conditioner variable type based on LCCP and TEWI approaches. *Res. Eng.* **21**. DOI:10.1016/j.rineng.2024.101806.
30. Suresh R., Saladi JK. and Datta SP. (2025). Energy, exergy and environmental life cycle assessment on the valorization of an ejector integrated CCHP system with six sustainable refrigerants. *Energy* **317**. DOI:10.1016/j.energy.2025.134664
31. Wang J., Yang Y., Mao T, et al. (2015). Life cycle assessment (LCA) optimization of solar-assisted hybrid CCHP system. *Appl. Energy* **146**:38–52. DOI:10.1016/j.apenergy.2015.02.056
32. Liu C., He C., Gao H, et al. (2013). The environmental impact of organic Rankine cycle for waste heat recovery through life-cycle assessment. *Energy* **56**:144–154. DOI:10.1016/j.energy.2013.04.045
33. Guo H., Wang H., He W, et al. (2025). C-P Diagram: A new thermodynamic analysis tool characterizing thermal cycles through geometric symmetry. *Innov. Energy* **2**. DOI:10.59717/j.xinn-energy.2025.100117.
34. Suresh R. and Datta SP. (2022). Drop-in Replacement of Conventional Automotive Refrigeration System to Hybrid-Ejector System with Environment-Friendly Refrigerants. *Energy Conver. Manag.* **266**. DOI:10.1016/j.enconman.2022.115819
35. Wang J., Dai Y. and Sun Z. (2009). A theoretical study on a novel combined power and ejector refrigeration cycle. *Int. J. Refrig.* **32**:1186–1194. DOI:10.1016/j.ijrefrig.2009.01.021

FUNDING AND ACKNOWLEDGMENTS

This work was primarily supported by the National Natural Science Foundation of China (Nos. 52206217 and U22B20112). T.Y. acknowledges the generous support from the National Key Laboratory of Multi–Perch Vehicle Driving Systems (No. QDXT-NY-202407-12). Academic Papers of the 28th Annual Meeting of the China Association for Science and Technology.

AUTHOR CONTRIBUTIONS

Tao Yang: Conceptualization, Software, Writing – Original Draft. Junbang Yao: Methodology, Writing–Original Draft; Xiaojing Li: Writing–Review & Editing, Supervision; Qibin Li: Validation, Writing–Review & Editing; Baomin Dai: Validation, Writing–Review & Editing; Yulong Song: Investigation, Software; Yifan Zhang: Validation, Software; Zilong Wang: Investigation, Conceptualization; Shuang Wang: Investigation, Conceptualization; Jian Li: Conceptualization, Formal Analysis; Jun Shen: Supervision.

DECLARATION OF INTERESTS

The authors declare that they have no known competing financial interests or personal relationships that could have appeared to influence the work reported in this paper.

DATA AND CODE AVAILABILITY

Data will be made available on request.